GEOLOGICAL JOURNAL
Geol. J. **41**: 49–59 (2006)
Published online 25 October 2005 in Wiley InterScience (www.interscience.wiley.com). DOI: 10.1002/gj.1032

High-pressure mineral assemblage in granitic rocks from continental units, Alpine Corsica, France

ALESSANDRO MALASOMA[1], MICHELE MARRONI[1,2], GIOVANNI MUSUMECI[1,2] and LUCA PANDOLFI[1,2]*

[1]*Dipartimento di Scienze della Terra, Universita' di Pisa, 56126 Pisa, Italy*
[2]*Istituto di Geoscienze e Georisorse, CNR, 56126 Pisa, Italy*

The Popolasca–Francardo area of northern Corsica contains an assemblage of continental tectonic units affected by an Alpine deformation. In one of these units, Unit II, previously regarded as weakly metamorphosed, a metamorphic mineral assemblage characterized by sodic amphibole, phengite, quartz, albite and epidote has been found in an aplite dyke that cuts the dominant granitoids. Peak-metamorphic temperature and pressure conditions of 300–370°C and 0.50–0.80 GPa, respectively, have been determined. This finding indicates that a continuous belt of continental slices, characterized by high-pressure, low-temperature metamorphism of Tertiary age, extends from the Tenda Massif in the north to the Corte area in the south, thus placing additional constraints on the tectonic evolution of Alpine Corsica. Copyright © 2005 John Wiley & Sons, Ltd.

Received 21 December 2004; revised version received 17 June 2005; accepted 17 July 2005

KEY WORDS high-pressure/low-temperature metamorphism; deformation; continental tectonic units; Alpine Corsica

1. INTRODUCTION

In Alpine Corsica, pervasive deformation associated with high-pressure/low-temperature (HP/LT) metamorphism has been recognized not only in oceanic units, but also in tectonic slices derived from the continental margin of the European plate. HP/LT metamorphism in the continental units has been long recognized and reported in the literature (e.g. Amaudric du Chaffault *et al.* 1976), but it has generally been under-evaluated, not only with respect to the pressure–temperature (P–T) conditions of the climax, but also with respect to the extent of the units affected by this metamorphism. Recently, Tribuzio and Giacomini (2002) and Molli and Tribuzio (2004) have demonstrated that the rocks of the Tenda continental massif experienced higher pressures than previously suggested. In this paper, we use detailed geological mapping, structural analysis and thermobarometry to provide further evidence for HP/LT metamorphism in Alpine Corsica. Our data illustrate that HP/LT metamorphism is more widespread than previously reported, and that it also affects some units hitherto reported as unmetamorphosed or weakly metamorphosed in the geological maps of Alpine Corsica (Rossi *et al.* 1994).

2. GEOLOGICAL SETTING

The island of Corsica can be divided into two distinct geological domains, Hercynian and Alpine Corsica (Figure 1). The western domain (Hercynian Corsica) is represented mainly by Carboniferous to Permian granitoids

* Correspondence to: M. Marroni, Dipartimento di Scienze della Terra, Universita' degli Studi di Pisa, S. Maria, 53, 56126 Pisa, Italy.
E-mail: marroni@dst.unipi.it

Contract/grant sponsor: Italian National Research Council.
Contract/grant sponsor: Italian Ministry for University and Scientific and Technological Research.

Copyright © 2005 John Wiley & Sons, Ltd.

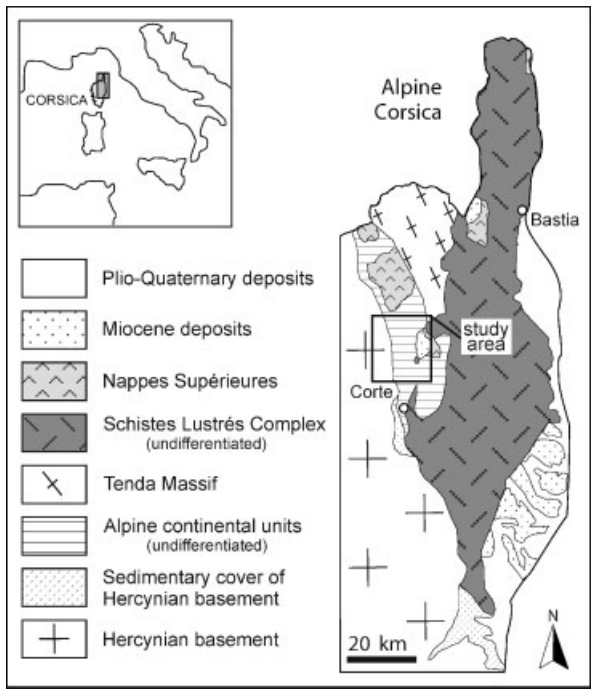

Figure 1. Tectonic sketch map of Alpine Corsica.

intruded into a Palaeozoic basement, with remnants of a sedimentary cover ranging in age from Late Carboniferous?–Jurassic to Late Eocene. The eastern domain (Alpine Corsica) consists of a complex stack of tectonic units derived from both oceanic and continental domains (e.g. Durand-Delga 1984). The oceanic units are considered to be remnants of the Liguria–Piemont oceanic basin (i.e. part of western Tethys), which developed between the European and Adriatic continental margins during the Triassic rifting and Jurassic spreading phases. From 'middle' Cretaceous times onwards, convergence affected the Liguria–Piemont oceanic basin leading to intra-oceanic subduction of oceanic lithosphere followed by continental collision, the latter continuing to the Late Eocene (e.g. Malavieille *et al.* 1998; Michard and Martinotti 2002). Starting in the Early Oligocene, compressional tectonics in Corsica was replaced by large-scale extension, resulting in collapse of the previously overthickened orogenic wedge (Jolivet *et al.* 1991).

The subduction-related tectonic events are well recorded in the Schistes Lustrés Complex, which includes both ophiolitic and continental sequences that were deformed and metamorphosed under HP/LT conditions. At the top of the Schistes Lustrés Complex, an assemblage of very low-grade metamorphic units (Nappes Supérieures) crops out, mainly represented by ophiolitic units (the Balagne, Nebbio and Pineto-Tribbio units). The Schistes Lustrés Complex is underlain by several tectonic units (the S. Lucia Nappe, Caporalino-S. Angelo Nappe, Palasca Unit, Corte Units and Tenda Massif) that are considered to be fragments of the European continental margin. These units consist of slices of Permian to 'middle' Eocene sedimentary cover associated with remnants of Palaeozoic basement, and were strongly affected by Alpine tectonics. Most of these units are regarded as weakly metamorphosed, the exceptions being the Tenda Massif, which underwent epidote–blueschist-facies metamorphism at *c*. 45 Ma (Brunet *et al.* 2000; Tribuzio and Giacomini 2002), and the Corte slices, which record low-grade blueschist-facies metamorphism (Amaudric du Chaffault *et al.* 1976; Bézert and Caby 1988). The contacts between the tectonic units of Alpine Corsica are sealed by Miocene (Burdigalian–Langhian) sedimentary basins which crop out in the Saint Florent and Francardo areas.

Copyright © 2005 John Wiley & Sons, Ltd.

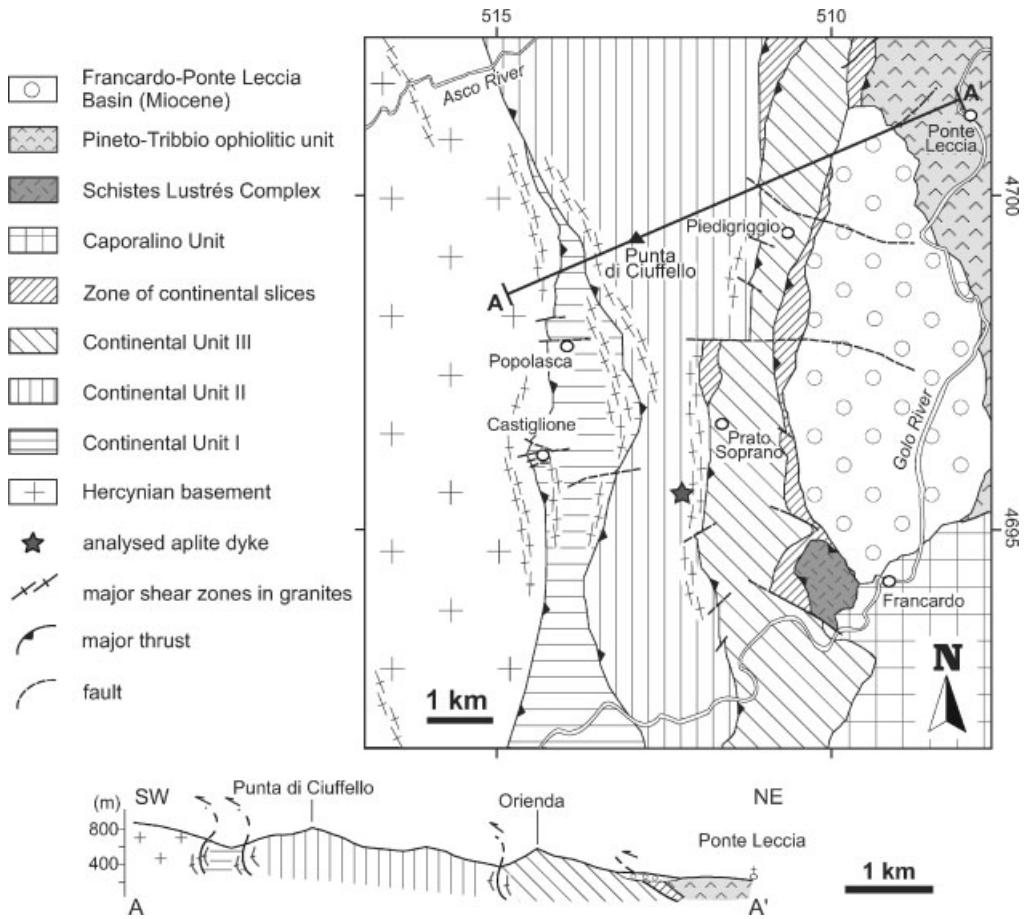

Figure 2. Tectonic sketch map and schematic cross-section of the study area. The location of the cross-section is indicated by the heavy line (A–A^{I}) in the sketch map.

3. GEOLOGICAL OUTLINE OF THE STUDY AREA

The study area is located between the Asco and Golo rivers in northern Corsica, along the boundary between Hercynian and Alpine Corsica (Figure 2). This area is characterized by the occurrence of three stacked tectonic units, each composed of slices of continental basement and its sedimentary cover, that have been thrust onto the Hercynian basement. These units are, in turn, overlain by two oceanic units, represented by the Schistes Lustrés Complex (a HP/LT metamorphic unit with an Inzecca Unit-type sedimentary cover) as well as the Pineto–Tribbio ophiolitic unit (a very low-grade metamorphic unit, cf. Balagne Nappe). Weakly deformed Lower Miocene conglomerates and sandstones of the Francardo–Ponte Leccia Basin seal all the contacts between the stacked tectonic units.

According to the 1:50 000 BRGM map (Rossi *et al.* 1994), the continental tectonic units are bounded by north–south-trending shear zones (Figure 2). In the western part of the study area, the shear zones are subvertical, whereas in the eastern part they dip gently eastwards. The westernmost unit, Unit I (called the *domaine autochtone* in the BRGM map), consists of an assemblage of continental slices, including both Hercynian granites (Permian) and Permo-Mesozoic to 'middle' Eocene sedimentary cover. This unit crops out along a narrow, north–south-trending belt where the 'middle' Eocene metapelites and the Hercynian granites record a polyphase deformation of Alpine age characterized by low-grade HP/LT metamorphism ($T = 250$–$350°C$, $P = 0.40$–0.55 GPa) (Bézert and Caby 1988). The intermediate unit, Unit II (called the *domaine parautochtone* in the BRGM map) consists

Copyright © 2005 John Wiley & Sons, Ltd.

of Permian Hercynian granites with remnants of their sedimentary cover. The easternmost unit, Unit III (called the *domaine prépiémontais* in the BRGM map) consists of a very thick Permian to Jurassic (possibly to Tertiary) sedimentary cover associated with remnants of Palaeozoic basement (Roches Brunes Formation). The sedimentary cover of Unit III has recorded an Alpine polyphase deformation, that can be correlated with the deformation recognized in Unit I.

4. DEFORMATION IN UNIT II

Unit II records a polyphase Alpine deformation history, consisting of three superposed deformation phases, here referred to as D1, D2 and D3.

The D1 phase is characterized by heterogeneous deformation with development of shear zones along the boundaries with the other units. Within shear zones, granites show a cataclastic–mylonitic deformation. Two main shear zones are recognized (Figure 2): the first one, *c*. 150 m thick, is located along the western margin over a length of *c*. 3.5 km along the contact with Unit I and the 'autochthonous domain'. The second shear zone, *c*. 100 m thick, has been recognized in the eastern margin. It crops out in the Prato Soprano area over a length of *c*. 3 km along the contact with Unit III. Within the shear zones, intrusive rocks are characterized by a N–S-trending penetrative and continuous foliation, parallel to the boundaries of Unit II (Figure 3). The mineral lineation on the foliation plane is defined by quartz ribbons and elongated mineral grains and it plunges moderately towards the E and NE. The attitudes of foliation and lineation are strongly influenced by subsequent deformation phases, in particular D3 (see below). The distribution of mineral lineations, after restoration of the D3 folds, is shown in Figure 3. Outside the shear zones, the intrusive rocks preserve an igneous texture and lack foliation.

The sheared granites display a foliation marked by aligned quartz ribbons and thin lepidoblastic layers of phyllosilicate (white mica + chlorite). When seen in thin section (Figure 4), these rocks can be classified as protomylonites and mylonites according to the matrix volume, which is in the range *c*. 50–70% (Sibson 1977). K-feldspar and quartz porphyroclasts are embedded in a fine-grained, foliated matrix composed of thin lepidoblastic layers of white mica and chlorite, aggregates of quartz and albite neoblasts, and Fe-oxides. The quartz porphyroclasts are characterized by low-temperature crystal–plastic deformation with undulose extinction, deformation lamellae and grain boundary migration. In contrast, the feldspar porphyroclasts are affected by brittle–ductile intracrystalline deformation, characterized by randomly orientated microfractures and microfaults associated with undulose extinction and replacement by albite (Figure 4). Kinematic indicators such as σ-type asymmetric strain fringes

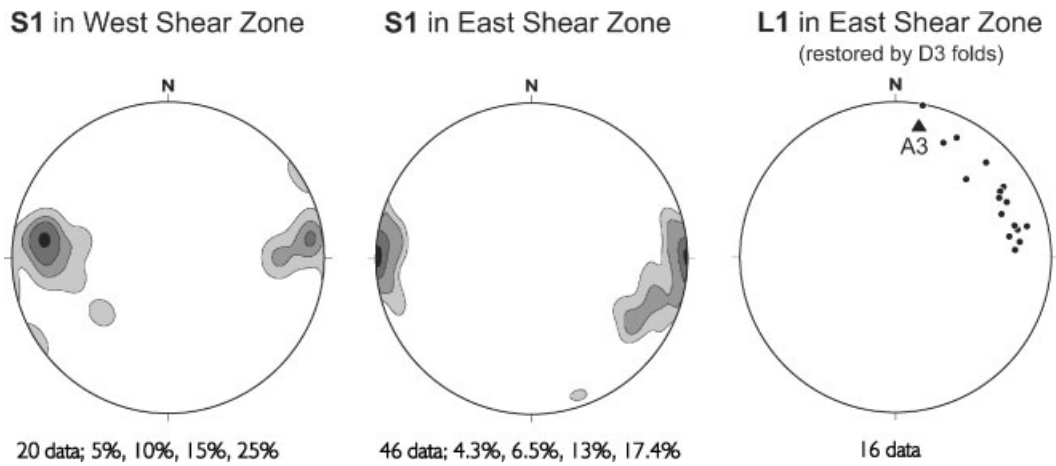

Figure 3. Stereographic representation (lower hemisphere, equal-area projection) of tectonic fabrics in Unit II ductile shear zones: (left) S1 foliation in the western shear zone; (centre) S1 foliation in the eastern shear zone; (right) L1 lineation in the eastern shear zone, after restoration of the effects of D3 folding.

Copyright © 2005 John Wiley & Sons, Ltd.

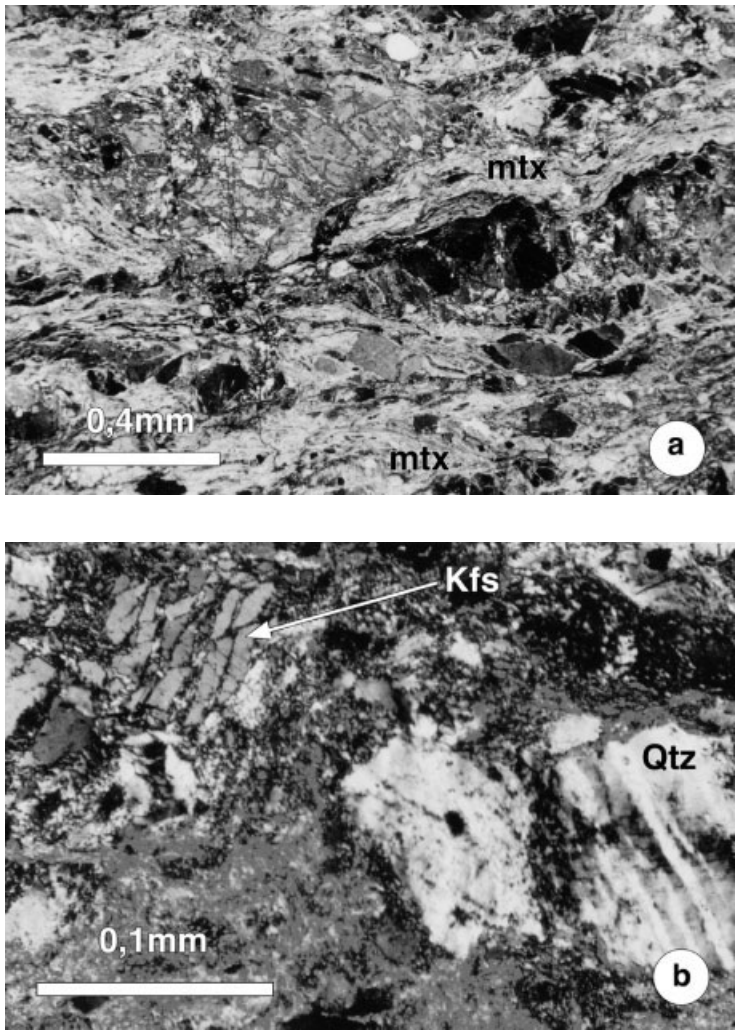

Figure 4. Microstructures related to the D1 deformation phase in Unit II granites. (**a**) Quartz and K-feldspar porphyroclasts in a fine-grained foliated (S1 foliation) matrix (mtx). Crossed polars. (**b**) Deformation lamellae and undulose extinction in quartz porphyroclast (Qtz) and microfractures in a K-feldspar porphyroclast (Kfs). Crossed polars.

around quartz and feldspar porphyroclasts indicate a top-to-the-SW sense of shear. According to Simpson (1985) and Pryer (1993), the microstructures recognized in quartz and feldspar porphyroclasts indicate that deformation developed at temperatures in the range 300–370°C, consistent with the upper limit of brittle deformation in feldspar.

A second deformation phase (D2) is represented by a brittle deformation superimposed on both deformed and undeformed granitoid bodies. At the mesoscopic scale, the granites display a pervasive cataclastic fabric. In thin section, the cataclasites are characterized by a well-developed fracture network affecting both quartz and feldspar porphyroclasts. Fractures are generally filled with microcrystalline aggregates of white mica, quartz and calcite. The brittle deformation in quartz grains indicates temperatures lower than 300°C.

A third deformation phase (D3) is represented by a map-scale fold that affects all the units cropping out in the study area. In Unit II, the D3 phase is responsible for the vertical attitude of the shear zones produced during D1 (Figure 2). On a small scale, the D1 foliation is weakly crenulated by structures produced during D3. Mesoscopic folds related to the D3 phase are rarely observed.

Copyright © 2005 John Wiley & Sons, Ltd.

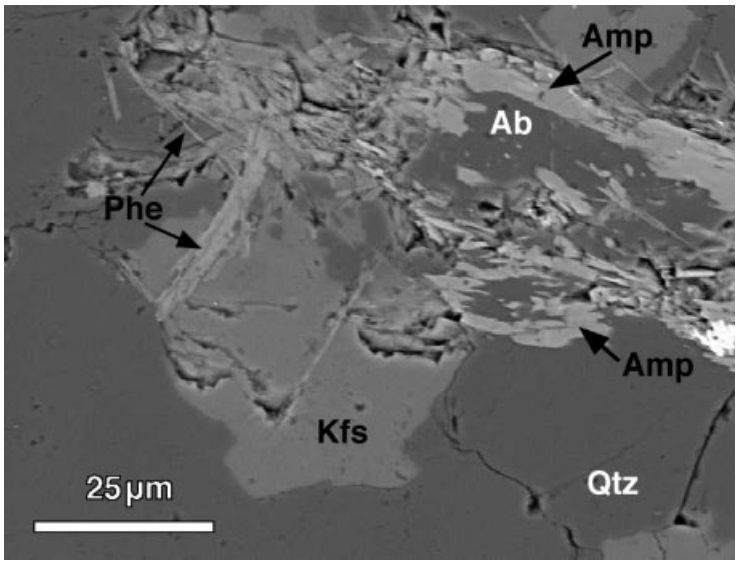

Figure 5. SEM image of the metamorphic mineral assemblage in the analysed aplite dyke in Unit II. Ab, albite; Amp, Na-amphibole; Kfs, K-feldspar; Phe, phengite; Qtz, quartz.

5. PEAK METAMORPHIC P–T CONDITIONS IN UNIT II

To estimate pressure–temperature (P–T) conditions during the metamorphic peak (D1 phase) in Unit II, information is provided by a metamorphic mineral assemblage found in an aplite dyke that cuts undeformed Hercynian granites SW of Prato di Giovellina (UTM coordinates: $X = 512.595$, $Y = 4695.620$). The host rock is a typical coarse-grained, calc-alkaline, leucocratic granite of Permian age. These granites are very rich in quartz and K-feldspar and are characterized by a very low content in femic minerals (mostly biotite). The aplite dyke is a fine-grained, phaneritic, leucocratic granitic rock composed almost entirely of quartz and K-feldspar, with minor amounts of Ca-amphibole and Fe-oxides. The peak-metamorphic mineral assemblage developed within a very fine-grained matrix between the quartz and K-feldspar grains. This assemblage comprises recrystallized Na-amphibole, phengite, quartz, albite and epidote (Figure 5). The Na-amphibole almost totally replaces the magmatic Ca-amphibole and preserves an original isotropic texture, typical of a static growth. Aggregates of fine-grained quartz, albite and phengite neoblasts have grown around the Na-amphibole crystals.

Chemical analyses of coexisting minerals within the metamorphic assemblages were obtained using a JEOL JXA-8600 electron microprobe, equipped with four wavelength-dispersive spectrometers, at the Istituto di Geoscienze e Georisorse, CNR, Firenze, Italy. Operating conditions were 15 kV accelerating voltage, 10 nA beam current, and beam spots between 1 and 10 µm in diameter. The largest spots were used on alkali-rich minerals, to avoid Na-K volatilization. Additional analyses were carried out using a Philips XL30 scanning electron microscope (SEM) system coupled with the EDAX-DX4 energy dispersive micro-analytical system (Department of Earth Sciences, University of Pisa).

5.1. Amphibole

Because of the small sizes of the amphibole crystals (widths *c*. 10 µm), it was not possible to make compositional traverses across individual crystals to detect intra-crystalline variations in chemical composition, such as core-to-rim zonation. Thus, each analysis reported in Table 1 represents a different crystal within the same rock sample. For the analysed sodic amphiboles, structural formulae were calculated assuming 23 oxygens, and the classification of Leake *et al*. (1997) was adopted. Site assignment and ferric iron contents were calculated using the scheme

Copyright © 2005 John Wiley & Sons, Ltd.

Table 1. Representative microprobe analyses (wt%) of Na-amphiboles. Structural formulae calculated assuming 23 oxygens per anhydrous formula unit

	Amp 1	Amp 2	Amp 3	Amp 4	Amp 5	Amp 6	Amp 7	Amp 8	Amp 9	Amp 10	Amp 11
SiO_2	53.18	53.26	52.46	50.15	53.29	53.52	53.36	51.73	55.81	53.87	55.44
TiO_2	—	0.12	0.12	0.18	0.09	—	—	4.70	0.11	0.54	0.06
Al_2O_3	2.00	2.36	1.76	3.96	2.52	2.22	1.39	1.36	1.65	1.25	1.41
Cr_2O_3	—	—	—	0.06	—	—	—	—	—	—	—
FeO	28.38	24.50	25.44	28.64	28.35	26.63	27.69	22.33	24.23	23.46	23.85
MnO	—	—	0.09	—	0.13	—	—	0.16	0.22	0.27	0.15
MgO	5.53	7.23	6.80	5.40	5.43	6.26	5.87	8.79	8.78	8.53	8.98
CaO	0.10	0.43	0.30	0.24	0.16	0.31	0.24	0.61	0.13	0.49	0.12
Na_2O	7.43	7.01	7.05	6.12	7.08	7.22	7.10	6.82	7.39	6.67	7.41
K_2O	0.10	0.18	0.08	0.70	0.14	0.12	0.09	0.10	0.04	0.13	0.08
Total	96.72	95.09	94.10	95.45	97.19	96.28	95.74	96.60	98.36	95.21	97.50
Cations											
Si	7.950	7.961	7.960	7.737	7.926	7.965	7.991	7.789	7.970	7.970	7.977
Al^{IV}	0.050	0.039	0.040	0.263	0.074	0.035	0.009	0.211	0.030	0.030	0.023
Sum T	*8.000*	*8.000*	*8.000*	*8.000*	*8.000*	*8.000*	*8.000*	*8.000*	*8.000*	*8.000*	*8.000*
Al^{VI}	0.302	0.377	0.275	0.457	0.367	0.354	0.236	0.030	0.248	0.188	0.216
Fe^{3+}	1.378	1.304	1.419	0.864	1.321	1.361	1.588	0.174	1.567	1.497	1.600
Ti	0.000	0.013	0.014	0.021	0.010	0.000	0.000	0.532	0.012	0.060	0.006
Cr	0.000	0.000	0.000	0.007	0.000	0.000	0.000	0.000	0.000	0.000	0.000
Mg	1.232	1.611	1.538	1.242	1.204	1.389	1.310	1.973	1.869	1.881	1.926
Fe^{2+}	2.087	1.695	1.754	2.409	2.098	1.896	1.866	2.291	1.304	1.373	1.251
Mn	0.000	0.000	0.000	0.000	0.000	0.000	0.000	0.000	0.000	0.000	0.000
Sum C	*5.000*	*5.000*	*5.000*	*5.000*	*5.000*	*5.000*	*5.000*	*5.000*	*5.000*	*5.000*	*5.000*
Mg	0.000	0.000	0.000	0.000	0.000	0.000	0.000	0.000	0.000	0.000	0.000
Fe^{2+}	0.082	0.064	0.054	0.422	0.107	0.057	0.015	0.347	0.022	0.032	0.019
Mn	0.000	0.000	0.012	0.000	0.016	0.000	0.000	0.020	0.027	0.034	0.018
Ca	0.016	0.069	0.049	0.040	0.025	0.049	0.039	0.098	0.020	0.078	0.018
Na	1.902	1.867	1.885	1.538	1.851	1.893	1.947	1.534	1.931	1.857	1.944
Sum B	*2.000*	*2.000*	*2.000*	*2.000*	*2.000*	*2.000*	*2.000*	*2.000*	*2.000*	*2.000*	*2.000*
Na	0.252	0.164	0.189	0.293	0.190	0.190	0.115	0.457	0.115	0.057	0.123
K	0.019	0.034	0.015	0.138	0.027	0.023	0.017	0.019	0.007	0.025	0.015
Sum A	*0.271*	*0.199*	*0.204*	*0.430*	*0.217*	*0.213*	*0.132*	*0.476*	*0.122*	*0.081*	*0.137*
Total	15.271	15.199	15.204	15.430	15.217	15.213	15.132	15.476	15.122	15.081	15.137

—, Below detection limit.

proposed by Schumacher in Leake *et al.* (1997). The sodic amphiboles are mostly riebeckite with $Mg/(Mg + Fe^{2+})$ ratios ranging from 0.30 to 0.58 (compositions close to the magnesio-riebeckite field) and are characterized by Si contents close to the maximum of 8.0 per formula unit (Table 1; Figure 6).

5.2. Phengite

The small grain size of the phengites also precluded study of intracrystalline variations in composition, so each analysis reported in Table 2 is from a different crystal within the same rock sample. Phengite structural formulae were calculated assuming 11 oxygens and all Fe as Fe^{2+}. Phengites have high celadonite contents, as indicated by high Si, Mg and Fe (Table 2) relative to muscovite.

The celadonite content of phengite is dependent mainly on pressure (Velde 1967) and forms the basis of a popular geobarometer in which Si isopleths have been calculated for phengite coexisting with K-feldspar, phlogopite, quartz and water in the K_2O–MgO–Al_2O_3–SiO_2–H_2O end-member system (Massonne and Szpurka 1997).

Copyright © 2005 John Wiley & Sons, Ltd.

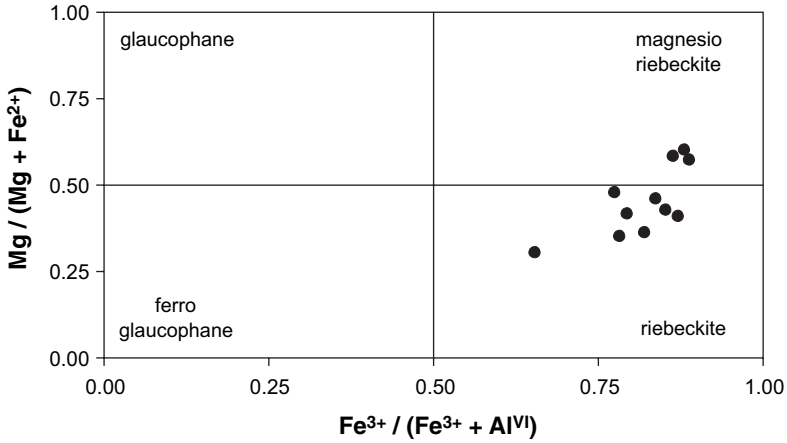

Figure 6. Composition of sodic amphiboles, using the classification of Leake *et al.* (1997).

This geobarometer can be applied to the Unit II meta-aplite dyke, as the analysed phengites have high celadonite contents. However, the lack of phlogopite (or biotite) in the assemblage means that the method yields only minimum pressure estimates (Tribuzio and Giacomini 2002). The analysed phengites have Si contents of between 3.42 and 3.65 atoms per formula unit (a.p.f.u.) with a maximum frequency of 3.50 a.p.f.u. (Table 2). If, as is likely, a small proportion of the Fe in phengite is Fe^{3+}, there would be a slight decrease in the Si content, typically <0.1 a.p.f.u., relative to the Fe^{3+}-free case.

Table 2. Representative microprobe analyses (wt%) of phengites. Structural formulae calculated assuming 11 oxygens per anhydrous formula unit with all Fe as Fe^{2+}

	Phe 1	Phe 2	Phe 3	Phe 4	Phe 5	Phe 6	Phe 7	Phe 8	Phe 9	Phe 10	Phe 11	Phe 12
SiO_2	52.36	52.24	51.55	49.99	50.88	51.02	49.93	50.7	50.81	49.05	48.72	49.48
TiO_2	—	—	0.29	0.16	0.75	0.55	1.42	0.46	0.57	0.59	0.60	0.80
Al_2O_3	20.17	18.65	21.20	23.92	20.16	21.02	20.63	19.27	19.96	20.20	19.19	19.22
FeO	7.17	13.21	10.85	6.22	9.74	8.80	8.49	9.00	8.41	8.72	12.02	9.40
MnO	—	—	0.08	0.18	0.07	0.07	—	0.07	—	—	0.09	—
MgO	4.82	1.54	2.89	3.95	4.50	4.64	4.27	4.62	4.31	4.36	4.50	4.57
CaO	0.04	—	—	—	0.06	—	—	0.04	—	0.04	0.05	0.04
Na_2O	—	—	—	—	—	—	—	—	—	—	—	0.09
K_2O	10.77	10.16	9.34	10.79	8.66	8.33	9.65	10.14	9.16	10.50	9.80	9.91
Total	95.33	95.80	96.20	95.21	94.82	94.43	94.39	94.30	93.22	93.46	94.97	93.51
Cations												
Si	3.590	3.654	3.535	3.424	3.520	3.515	3.475	3.549	3.559	3.476	3.449	3.506
Al^{IV}	0.410	0.346	0.465	0.576	0.480	0.485	0.525	0.451	0.441	0.524	0.551	0.494
Sum Z	*4.000*	*4.000*	*4.000*	*4.000*	*4.000*	*4.000*	*4.000*	*4.000*	*4.000*	*4.000*	*4.000*	*4.000*
Al^{VI}	1.219	1.191	1.248	1.354	1.163	1.222	1.166	1.139	1.206	1.163	1.050	1.111
Ti	0.000	0.000	0.015	0.008	0.039	0.028	0.074	0.024	0.030	0.031	0.032	0.043
Fe^{2+}	0.411	0.772	0.622	0.356	0.563	0.507	0.494	0.527	0.492	0.517	0.711	0.557
Mn	0.000	0.000	0.005	0.010	0.004	0.004	0.000	0.004	0.000	0.000	0.005	0.000
Mg	0.492	0.160	0.295	0.403	0.464	0.476	0.443	0.482	0.450	0.460	0.475	0.482
Sum Y	*2.122*	*2.124*	*2.185*	*2.132*	*2.233*	*2.237*	*2.177*	*2.176*	*2.178*	*2.171*	*2.273*	*2.192*
Ca	0.003	0.000	0.000	0.000	0.004	0.000	0.000	0.003	0.000	0.003	0.004	0.003
Na	0.000	0.000	0.000	0.000	0.000	0.000	0.000	0.000	0.000	0.000	0.000	0.012
K	0.942	0.906	0.817	0.942	0.764	0.732	0.856	0.905	0.818	0.949	0.885	0.895
Sum X	*0.944*	*0.906*	*0.817*	*0.942*	*0.768*	*0.732*	*0.856*	*0.908*	*0.818*	*0.952*	*0.888*	*0.911*
Total	7.066	7.030	7.002	7.074	7.002	6.969	7.033	7.084	6.996	7.123	7.161	7.103

—, Below detection limit.

Copyright © 2005 John Wiley & Sons, Ltd.

Peak P–T conditions of metamorphism are constrained by the association of Na-amphibole + phengite + quartz + albite + epidote. In the studied meta-aplite, phengite coexists with sodic amphibole, albite, quartz and K-feldspar. In this assemblage the celadonite content of phengite is buffered by the equilibrium:

$$2NaAlSi_3O_8 + 3KMgAlSi_4O_{10}(OH)_2 = Na_2Mg_3Al_2Si_8O_{22}(OH)_2 + 3KAlSi_3O_8 + SiO_2 + 2H_2O \quad (1)$$

albite phengite sodic amphibole K-feldspar quartz fluid.

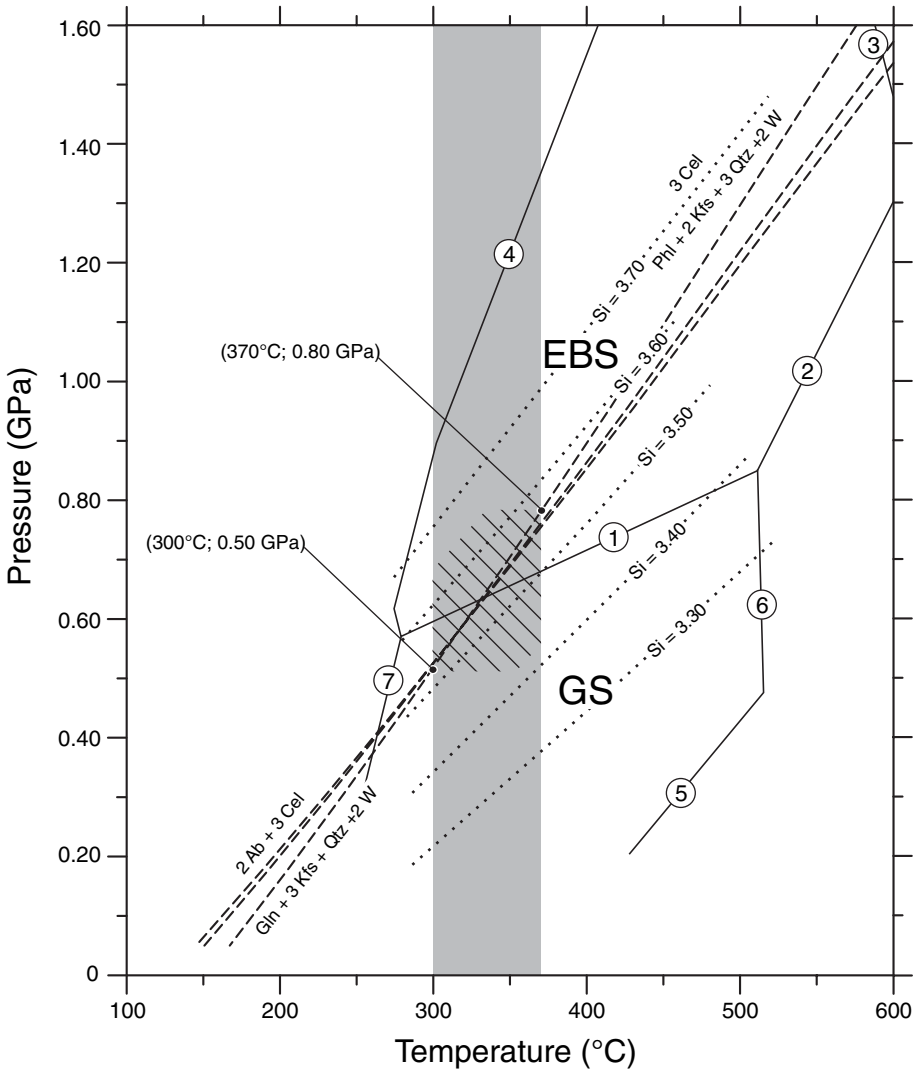

Figure 7. Estimated peak-metamorphic pressure/temperature conditions in Unit II (cross-hatched area). The reaction curves 2Ab + 3Cel = Gln + 3Kfs + Qtz + 2W (dashed lines) were calculated with the TWEEQ program (Berman 1991). The reaction curves 3Cel = Phl + 2Kfs + 3Qtz + 2W (Massonne and Szpurka 1997) are also shown (dotted lines). P–T grid for epidote–blueschist facies (continuous lines) following Na-amphibole composition no. 6 of Evans (1990). The shaded area represents the temperature range (300–370°C) constrained by the microstructures. Abbreviations: EBS, epidote–blueschist facies; GS, geenschist facies; 1, Gln + Czo + Qtz + W = Ab + Chl + Tr; 2, Gln + Czo + Qtz = Ab + Prp + Tr + W; 3, Gln + Czo = Jd + Di + Prp + Qtz + W; 4, Czo + Gln + Qtz + W = Lws + Di + Jd; 5, Chl + Czo + Qtz = An + Tr + W; 6, Chl + Czo + Qtz = Prp + Tr + W; 7, Pmp + Chl + Qtz = Czo + Tr + W; Ab, albite; An, anorthite; Cel, celadonite; Chl, chlorite; Czo, clinozoisite; Di, diopside; Gln, glaucophane; Jd, jadeite; Kfs, K-feldspar; Lws, lawsonite; Na-Amp, sodic amphibole; Phl, phlogopite; Pmp, pumpellyite; Prp, pyrope; Qtz, quartz; Tr, tremolite; W, water.

Copyright © 2005 John Wiley & Sons, Ltd.

The P–T position of this equilibrium, duly corrected for dilution of celadonite and glaucophane components in phengite and sodic amphibole, respectively, has been calculated using the TWEEQ program (Berman 1991); the thermodynamic data and the solid solution models are from Berman (1988, 1990) for all phases except K-white mica, for which the model of Parra *et al.* (2002) was used. The glaucophane activity (a_{Gln}) in the Na-amphibole was calculated using the formula of Evans (1990): $a_{Gln} = (X_{Na}{}^{M4})^2\,(al)^2\,(mg)^3$, where $X_{Na}{}^{M4}$ is the mole fraction of Na in the M4 structural site; $al = Al^{VI}/(Al^{VI} + Fe^{3+})$; $mg = Mg/(Mg + Fe^{2+})$. For the temperature range constrained by the study of microstructures in quartz and feldspar porphyroclasts (T = 300–370°C), the calculated equilibrium curve gives a pressure range between 0.50 and 0.80 GPa, close to the greenschist/epidote–blueschist metamorphic facies transition (Figure 7). Also, the Si-in-phengite geobarometer (Massonne and Szpurka 1997) provides a pressure minimum in the range 0.40–0.85 GPa, which is broadly consistent with the estimated pressure (Figure 7) given a likely uncertainty in the position of Equilibrium 1 of at least ±0.2 GPa. Summing up the available thermobarometric information, the metamorphic conditions can be determined as T = 300–370°C and P = 0.50–0.80 GPa (Figure 7).

6. CONCLUSIONS

The occurrence of Alpine polyphase deformation suggests that all the continental units between the Francardo–Ponte Leccia Basin and the autochthonous domain (Figure 2) were involved in the Alpine Orogeny. Moreover, the occurrence of a mineral assemblage characterized by sodic amphibole and phengite in the granitic rocks of Unit II (Popolasca–Francardo area, Figure 2), indicates that Alpine HP/LT metamorphism also affected this continental slice (previously regarded as weakly metamorphosed) with a metamorphic grade and P–T conditions similar to those observed in the underlying Unit I (Bézert and Caby 1988).

In the studied tectonic units, the deformation phases are older than Burdigalian (the age of the oldest deposits found in the Francardo–Ponte Leccia Basin), and according to Bézert and Caby (1988) the HP/LT metamorphism in Unit I is younger than 'middle' Eocene (the age of the flysch involved in the D1 deformation phase). According to geological data, the same age can be extended to the D1 phase recognized in Unit II. Thus, the D1, D2 and D3 phases can be regarded as ranging in age from Late Eocene to Early Miocene (Burdigalian).

As a whole, a continuous belt of continental slices characterized by HP/LT metamorphism of Tertiary age can be identified from the Tenda Massif to the Corte area. In these slices, the metamorphism ranges from low-grade blueschist facies (T = 300–370°C and P = 0.50–0.80 GPa; slices of Corte and Popolasca area) to epidote–blueschist facies (T = 300–500°C and P = 0.80–1.10 GPa; Tenda Massif). This picture supports the hypothesis that large portions of the Corsican continental basement were deformed under HP/LT metamorphic conditions during their involvement in the tectonics connected with Alpine subduction (Amaudric du Chaffault *et al.* 1976; Bézert and Caby 1988; Tribuzio and Giacomini 2002; Molli and Tribuzio 2004) and were subsequently juxtaposed against the metamorphic and non-metamorphic oceanic units during exhumation (e.g. Malavieille *et al.* 1998).

ACKNOWLEDGEMENTS

This research was supported by the Italian National Research Council (IGG, Istituto di Geoscienze e Georisorse, CNR Pisa) and by the Italian Ministry for University and Scientific and Technological Research (M.I.U.R.–COFIN). Reviews by GTR Droop substantially improved this paper.

REFERENCES

Amaudric du Chaffault S, Kienast JR, Saliot P. 1976. Répartition de quelques minéraux du métamorphisme alpin en Corse. *Bullettin de la Société Géologique de France* **7**: 149–154.

Berman RG. 1988. Internally-consistent thermodynamic data for stoichiometric minerals in the system Na_2O-K_2O-CaO-MgO-FeO-Fe_2O_3-Al_2O_3-SiO_2-TiO_2-H_2O-CO_2. *Journal of Petrology* **29**: 445–522.

Copyright © 2005 John Wiley & Sons, Ltd.

Berman RG. 1990. Mixing properties of Ca-Mg-Fe-Mn garnets. *American Mineralogist* **75**: 328–344.
Berman RG. 1991. Thermobarometry using multiequilibrium calculations: a new technique with petrologic applications. *Canadian Mineralogist* **29**: 833–855.
Bézert P, Caby R. 1988. Sur l'âge post-bartonien des évenements tectono-metamorphiques alpins en bordure orientale de la Corse cristalline (Nord de Corte). *Bullettin de la Société Géologique de France* **8**: 965–971.
Brunet C, Monié P, Jolivet L, Cadet JP. 2000. Migration of compression and extension in the Thyrrenian Sea, insights from 40Ar/39Ar ages on micas along a transect from Corsica to Tuscany. *Tectonophysics* **321**: 127–155.
Durand-Delga M. 1984. Principaux traits de la Corse Alpine et correlations avec les Alpes Ligures. *Memorie della Società Geologica Italiana* **28**: 285–329.
Evans BW. 1990. Phase relations of epidote-blueschists. *Lithos* **25**: 3–23.
Jolivet L, Daniel JM, Fournier M. 1991. Geometry and Kinematics of extension in Alpine Corsica. *Earth and Planetary Science Letters* **104**: 278–291.
Leake BE, Wooley AR, Arps CES, Birch WD, Gilbert MC, Grice JD, Hawthorne FC, Kato A, Kisch HJ, Krivivichev VG, Linthout K, Laird J, Mandarino JA, Maresch WV, Nickel EH, Rock NMS, Schumacher JC, Smith DC, Stephenson NCN, Ungaretti L, Whittaker E, Youzhi G. 1997. Nomenclature of amphiboles: Report of subcommittee on amphiboles of the International Mineralogical Association, commission on new minerals and mineral names. *Canadian Mineralogist* **35**: 219–246.
Malavieille J, Chemenda A, Larroque C. 1998. Evolutionary model for Alpine Corsica: mechanism for ophiolite emplacement and exhumation of high-pressure rocks. *Terra Nova* **10**: 317–322.
Massonne HJ, Szpurka Z. 1997. Thermodynamic properties of white micas on the basis of high-pressure experiments in the systems K_2O-MgO-Al_2O_3-SiO_2-H_2O and K_2O-FeO-Al_2O_3-SiO_2-H_2O. *Lithos* **41**: 229–250.
Michard A, Martinotti G. 2002. The Eocene unconformity of the Briançonnais domain in the French-Italian Alps, revisited (Marguareis massif, Cuneo); a hint for a Late Cretaceous–Middle Eocene frontal bulge setting. *Geodinamica Acta* **15**: 289–301.
Molli G, Tribuzio R. 2004. Shear zones and metamorphic signature of subducted continental crust as tracers of the evolution of the Corsica/Northern Apennine orogenic system. In *Flow Processes in Faults and Shear Zones*, Alsop GI, Holdsworth RE, McCaffrey KJW, Hand M (eds). Geological Society, London, Special Publication **224**: 321–335.
Parra T, Vidal O, Agard P. 2002. A thermodynamic model for Fe-Mg dioctahedral K white micas using data from phase-equilibrium experiments and natural pelitic assemblages. *Contributions to Mineralogy and Petrology* **143**: 706–732.
Pryer LL. 1993. Microstructures in feldspars from a major crustal thrust zone: the Grenville Front, Ontario, Canada. *Journal of Structural Geology* **15**: 21–36.
Rossi P, Durand-Delga M, Caron JM, Guieu G, Conchon O, Libourel G, Loye-Pilot MD, Olle JJ, Pequignot G, Potdevin JL, Rieuf M, Rodriguez G, Sedan O, Vellutini PJ, Rouire J. 1994. *Carte géologique de la France (1/50 000^e), feuille Corte (1110)*. BRGM: Orléans.
Sibson RH. 1977. Fault rocks and fault mechanisms. *Journal of the Geological Society of London* **133**: 191–213.
Simpson C. 1985. Deformation of granitic rocks across the brittle–ductile transition. *Journal of Structural Geology* **7**: 503–511.
Tribuzio R, Giacomini F. 2002. Blueschist facies metamorphism of peralkaline rhyolites from the Tenda crystalline massif (northern Corsica): evidence for involvement in the Alpine subduction event? *Journal of Metamorphic Geology* **20**: 513–526.
Velde B. 1967. Si^{+4} content of natural phengites. *Contributions to Mineralogy and Petrology* **14**: 250–258.

Scientific editing by Giles Droop

Copyright © 2005 John Wiley & Sons, Ltd.